



LUND UNIVERSITY

Nanoscale characterization of collagen structural responses to in situ loading in rat Achilles tendons

Silva Barreto, Isabella; Pierantoni, Maria; Hammerman, Malin; Törnquist, Elin; Le Cann, Sophie; Diaz, Ana; Engqvist, Jonas; Liebi, Marianne; Eliasson, Pernilla; Isaksson, Hanna

Published in:
Matrix Biology

DOI:
[10.1016/j.matbio.2022.11.006](https://doi.org/10.1016/j.matbio.2022.11.006)

2023

Document Version:
Peer reviewed version (aka post-print)

[Link to publication](#)

Citation for published version (APA):
Silva Barreto, I., Pierantoni, M., Hammerman, M., Törnquist, E., Le Cann, S., Diaz, A., Engqvist, J., Liebi, M., Eliasson, P., & Isaksson, H. (2023). Nanoscale characterization of collagen structural responses to in situ loading in rat Achilles tendons. *Matrix Biology*, 115, 32-47. <https://doi.org/10.1016/j.matbio.2022.11.006>

Total number of authors:
10

Creative Commons License:
CC BY-NC-ND

General rights

Unless other specific re-use rights are stated the following general rights apply:
Copyright and moral rights for the publications made accessible in the public portal are retained by the authors and/or other copyright owners and it is a condition of accessing publications that users recognise and abide by the legal requirements associated with these rights.

- Users may download and print one copy of any publication from the public portal for the purpose of private study or research.
- You may not further distribute the material or use it for any profit-making activity or commercial gain
- You may freely distribute the URL identifying the publication in the public portal

Read more about Creative commons licenses: <https://creativecommons.org/licenses/>

Take down policy

If you believe that this document breaches copyright please contact us providing details, and we will remove access to the work immediately and investigate your claim.

LUND UNIVERSITY

PO Box 117
221 00 Lund
+46 46-222 00 00

1 *Accepted version*

2 **Nanoscale characterization of collagen structural responses to *in situ***
3 **loading in rat Achilles tendons**

4 **Authors:** Isabella Silva Barreto¹, Maria Pierantoni¹, Malin Hammerman^{1,2}, Elin Törnquist¹,
5 Sophie Le Cann³, Ana Diaz⁴, Jonas Engqvist⁵, Marianne Liebi^{4,6,7}, Pernilla Eliasson^{2,8},
6 Hanna Isaksson¹

7

8 **Affiliations:**

9 ¹ Department of Biomedical Engineering, Lund University, Lund, Sweden

10 ² Department of Biomedical and Clinical Sciences, Linköping University, Linköping, Sweden

11 ³ CNRS, Univ Paris Est Creteil, Univ Gustave Eiffel, UMR 8208, MSME, F-94010 Créteil,
12 France

13 ⁴ Paul Scherrer Institut, Villigen PSI, Switzerland

14 ⁵ Division of Solid Mechanics, Lund University, Lund, Sweden

15 ⁶ Department of Physics, Chalmers University, Gothenburg, Sweden

16 ⁷ Center of X-ray Analytics, Empa, Swiss Federal Laboratories for Materials Science and
17 Technology, St.Gallen, Switzerland

18 ⁸ Department of Orthopaedics, Sahlgrenska University Hospital, Gothenburg, Sweden

19

20

21 ***To whom correspondence should be addressed:**

22 Professor Hanna Isaksson, PhD

23 Department of Biomedical Engineering

24 Lund University / LTH

25 Box 118, 221 00 Lund, Sweden

26 E-mail: hanna.isaksson@bme.lth.se

27

28 **Declarations of interest:** none

29 **ABSTRACT**

30 The specific viscoelastic mechanical properties of Achilles tendons are highly dependent on the
31 structural characteristics of collagen at and between all hierarchical levels. Research has been
32 conducted on the deformation mechanisms of positional tendons and single fibrils, but
33 knowledge about the coupling between the whole tendon and nanoscale deformation
34 mechanisms of more commonly injured energy-storing tendons, such as Achilles tendons,
35 remain sparse. By exploiting the highly periodic arrangement of tendons at the nanoscale, *in*
36 *situ* loading of rat Achilles tendons during small-angle X-ray scattering acquisition was used to
37 investigate the collagen structural response during load to rupture, cyclic loading and stress
38 relaxation. The fibril strain was substantially lower than the applied tissue strain. The fibrils
39 strained linearly in the elastic region of the tissue, but also exhibited viscoelastic properties,
40 such as an increased stretchability and recovery during cyclic loading and fibril strain relaxation
41 during tissue stress relaxation. We demonstrate that the changes in the width of the collagen
42 reflections could be attributed to strain heterogeneity and not changes in size of the coherently
43 diffracting domains. Fibril strain heterogeneity increased with applied loads and after the toe
44 region, fibrils also became increasingly disordered. Additionally, a thorough evaluation of
45 radiation damage was performed. In conclusion, this study clearly displays the simultaneous
46 structural response and adaption of the collagen fibrils to the applied tissue loads and provide
47 novel information about the transition of loads between length scales in the Achilles tendon.

48

49 **Keywords:** Achilles tendon, nanomechanics, collagen structure, small-angle X-ray scattering,
50 *in situ* loading

51

52

53 1 INTRODUCTION

54 Achilles tendons transduce forces from the gastrocnemius soleus muscle complex to
55 calcaneal bone, allowing energy efficient movement of the foot. Their viscoelastic mechanical
56 behavior and intrinsic properties are directly connected to their complex hierarchical structure
57 [1,2]. The main constituents of tendons are water (55-70 % of wet weight) and collagen (60-85
58 % of dry weight). The collagen type I molecules (approximately 300 nm long triple helices)
59 assemble into fibrils, organized in a quarter stagger arrangement at a periodic distance (d-
60 spacing) of approximately 67 nm. The d-spacing includes a gap region (space in-between
61 collagen molecules) and an overlap region (where collagen molecules overlap and are
62 crosslinked) [3]. This quarter-staggered arrangement of molecules makes up the sub-unit of
63 collagen [4,5]. The fibrils (~100 nm) assemble into fibers (~10 μm), that in turn assemble into
64 fascicles and subs-tendons (~500 μm), and together with the interfascicular matrix, ultimately
65 constitute the whole tendon. The mechanical properties and behavior of the whole tendon is a
66 result of optimization at and between these hierarchical levels [1,2]. Due to the complexity of
67 this relation, the strain transfer between different levels as well as the different deformation
68 mechanisms behind the tissue properties and behavior, are still not completely understood.

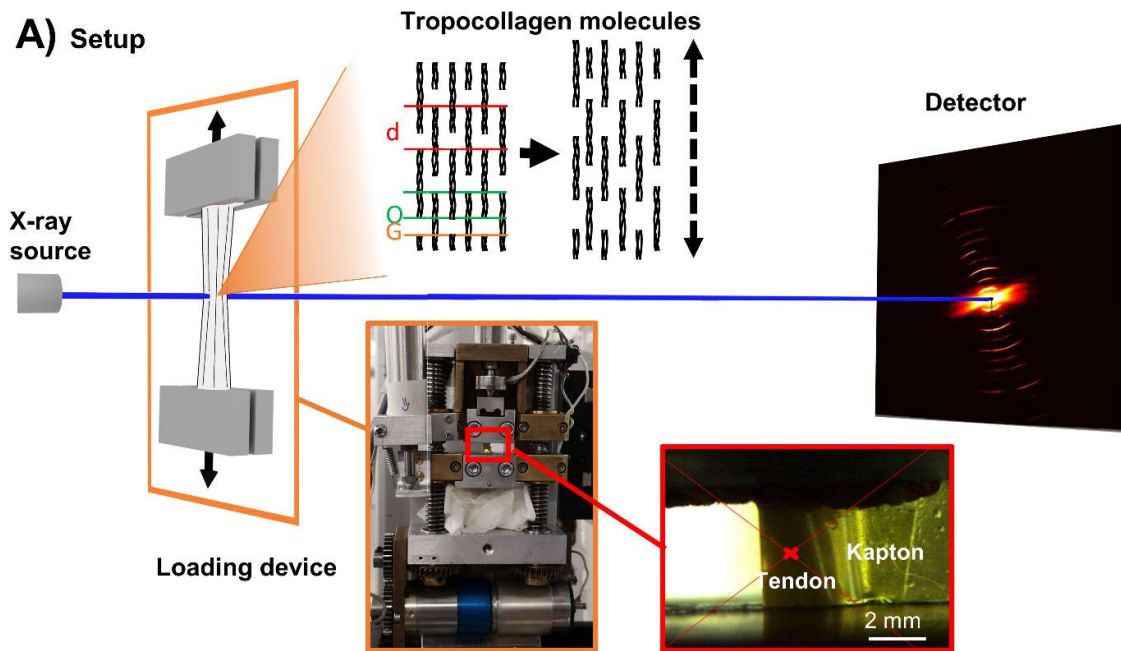
69 As collagen fibrils are arranged in a highly periodic arrangement, they can be probed using
70 X-ray diffraction techniques such as small- and wide-angle X-ray scattering (SAXS and
71 WAXS) [5-7]. Using synchrotron radiation, these techniques have been applied during *in situ*
72 loading, i.e. tensile loading of the full tendon while simultaneously conducting scattering
73 measurements, to assess real-time collagen deformation mechanisms, which has led to the
74 currently accepted concepts of fibril elongation through collagen molecule extension,
75 elongation of gap regions and relative sliding of adjacent molecules [7-11]. In these studies, the
76 fibril strain has been observed to be lower than the applied tissue strain, implying that strain is
77 being partitioned between length scales, very likely through interfibrillar sliding [12] or the

78 interfibrillar matrix supporting parts of the load ^[13]. At larger strains, there has been indications
79 of loss of intrafibrillar order ^[14], and macroscopic failure has been observed to be preceded by
80 interfibrillar sliding and damage ^[15]. In studies conducting mechanical testing of dissected
81 single fibrils, however, larger fibril strains between 11-27% have been observed ^[16-19], with
82 fibrils from Achilles tendons straining slightly less than e.g. tail tendons ^[18,19]. This indicates
83 that the fibrils themselves can deform substantially more than they do when interconnected and
84 assembled into larger functional units such as fascicles ^[8,9].

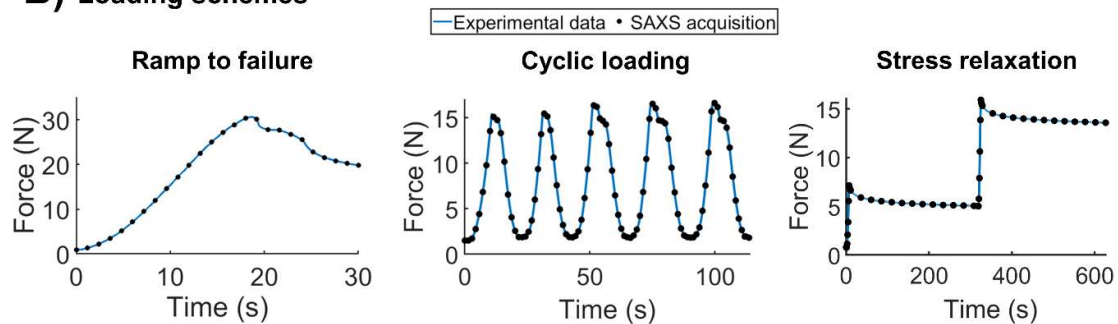
85 Despite the extensive research in the field of collagen mechanics, the characteristics and
86 timing of key aspects and events during collagen nano-response to loading remain debated, and
87 the relation to the tissue scale is not completely understood. Further, most studies have used
88 fascicles from the rat tail tendon as a model of collagen mechanics ^[5,7-11,13,20-22]. In addition to
89 fascicles not being representative of the whole tendon, tail tendons are positional tendons and
90 therefore experience the mechanical environment differently compared to energy-storing
91 tendons ^[23]. In the case of energy-storing tendons, the literature is sparse. The differences in
92 mechanical properties and response between positional and energy-storing tendons have been
93 highlighted in numerous studies ^[19,23-29]. For example, energy-storing tendons seem to rely
94 heavily on fiber reorganization and fibril relaxation during tissue stress relaxation ^[23] and
95 accumulate less fatigue induced fibril damage ^[28]. Contrariwise, positional tendons seemed to
96 have less capacity for this type of response and experience more plastic and accumulated fatigue
97 damage. However, it remains debated if these differences extend down to the single nanoscale
98 collagen fibril. While one study on single fibril mechanics showed similarities between collagen
99 fibrils from positional and energy-storing tendons despite their difference in cross-linking ^[18],
100 another study showed differences in both the single fibril response and in some mechanical
101 properties ^[19]. Thus, there is still a lack of knowledge regarding these processes and the relation

102 between length scales in complex energy-storing tendons such as the Achilles tendon, which is
103 one of the most commonly injured tendons in humans ^[30].

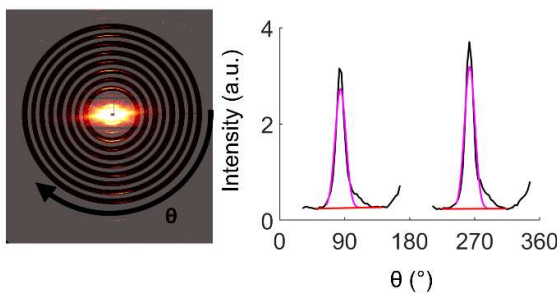
104 The aim of this study was to characterize collagen nano-structural deformation mechanisms
105 in rat Achilles tendons and to determine how changes in collagen fibril arrangement relate to
106 the tissue-level mechanical behavior. Specifically, we aimed to evaluate both elastic and
107 viscoelastic behaviors at the collagen fibril level vs the tissue scale. This was achieved through
108 a combination of SAXS and simultaneous *in situ* tensile loading to quantify structural response
109 at the nanoscale and to elucidate to what extent collagen fibrils align, stretch, slide, and fail in
110 response to different tissue loading protocols (Figure 1). Additionally, a radiation damage test
111 was conducted prior to mechanical testing to ensure that the repeated SAXS exposure would
112 not significantly affect the collagen structure.



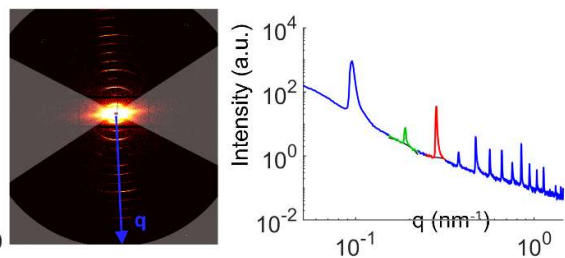
B) Loading schemes



C) Orientation analysis



D) Collagen analysis



113

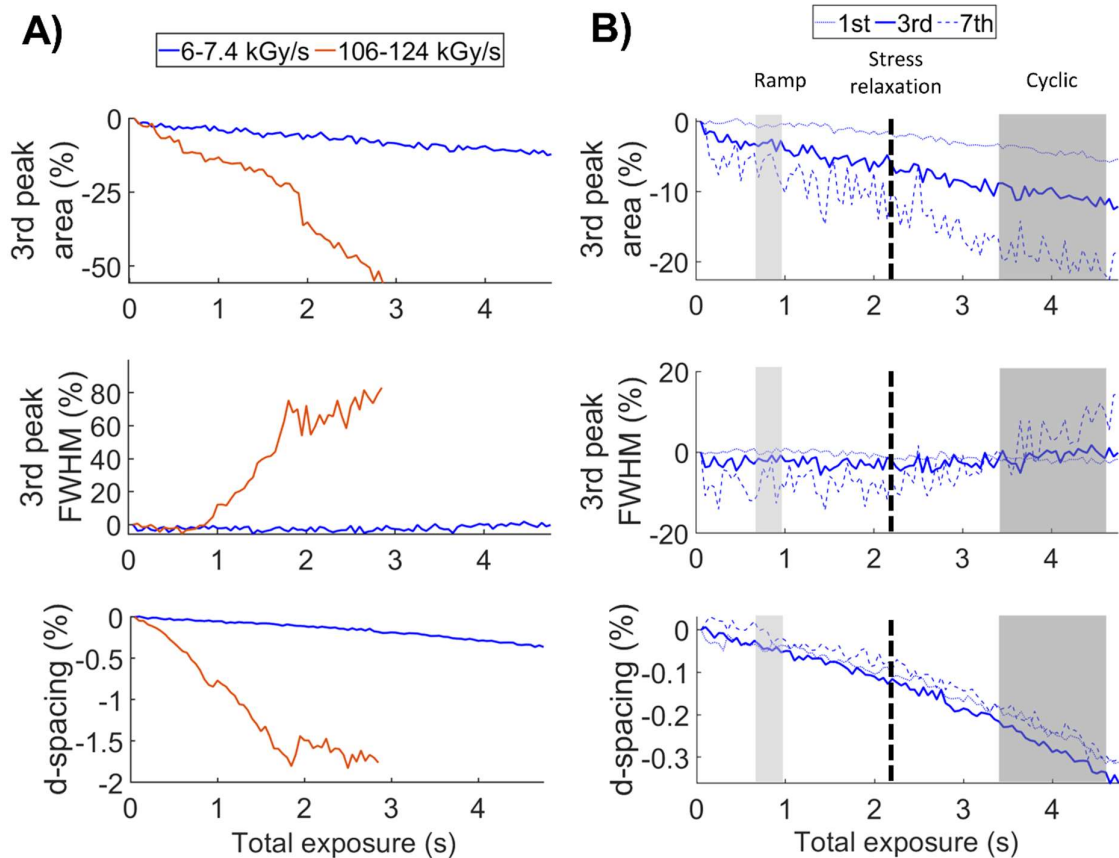
114 **Figure 1. Schematic figures of experiment.** A) Illustration of the combined SAXS and *in situ* loading setup, indicating the d-spacing (d), gap (G) and overlap (O) regions in the unstretched fibril state and how these change during loading. Picture showing the tendon mounted in the loading device and a representative zoom-in as visualized with the microscope, indicating the position for SAXS acquisition (red cross). B) Representative applied load curves. C) The q -regions used (not shaded) for obtaining the intensity as a function of angle $I(\theta)$ (black - smoothed data, purple - Gaussian fit, red - background). D) The q -region used (not shaded) for obtaining the intensity as a function of the q -vector $I(q)$ (blue), indicating the peaks originating from the 2nd (green) and 3rd reflection (red).

122

123 **3 RESULTS**

124 **3.1 Radiation damage**

125 During the radiation damage test conducted prior to the loading tests, the d-spacing and peak
126 area displayed a gradual decrease already from the first exposure (Figure 2.A). With a dose rate
127 of 106-124 kGy/s ($32 \times 20 \mu\text{m}^2$ beam size) (Figure 1.A), a severe change in strain heterogeneity
128 was observed after around 0.6 s of cumulated exposure, which corresponds to a total dose of
129 approximately 64-74 kGy. This dose level is slightly lower than previously reported values for
130 structural damage of collagen in breast tissue (approximately 100 kGy) ^[31]. In relation to this,
131 the total dose which initiated clear changes in the collagen structure in this study seemed
132 reasonable. Thus, a beam size of $150 \times 125 \mu\text{m}^2$ was chosen, which corresponded to a dose rate
133 of approximately 6-7.4 kGy/s. This resulted in an estimated total dose of 4.5-7 kGy during ramp
134 to failure, 13-16 kGy during stress relaxation and 21-34 kGy during cyclic loading (Figure 2.B).
135 Within the total doses for the different loading schemes, small structural changes occurred in
136 the collagen fibrils compared to the changes induced by loading. Thus, it was assumed that the
137 majority of the results from this study were not severely influenced by radiation damage.



138

139 **Figure 2. Radiation damage.** The effect of dose rate and total exposure time on some of the collagen structural
 140 parameters for one sample. A) Changes in collagen structural parameters for the two dose rates. A clear change in
 141 3rd peak FWHM is observed after 0.6 s. B) The effect on the 1st, 3rd and 7th meridional Bragg peaks from using a
 142 dose rate of 6-7.4 kGy/s, which was selected for the remaining study. The shaded areas (vertical bars) indicate the
 143 range of maximum exposure during the mechanical tests. For instance, exposure time ranged from 0.6 to 1.2 s
 144 among specimens during the ramp to failure tests.

145

146 3.2 Ramp to failure

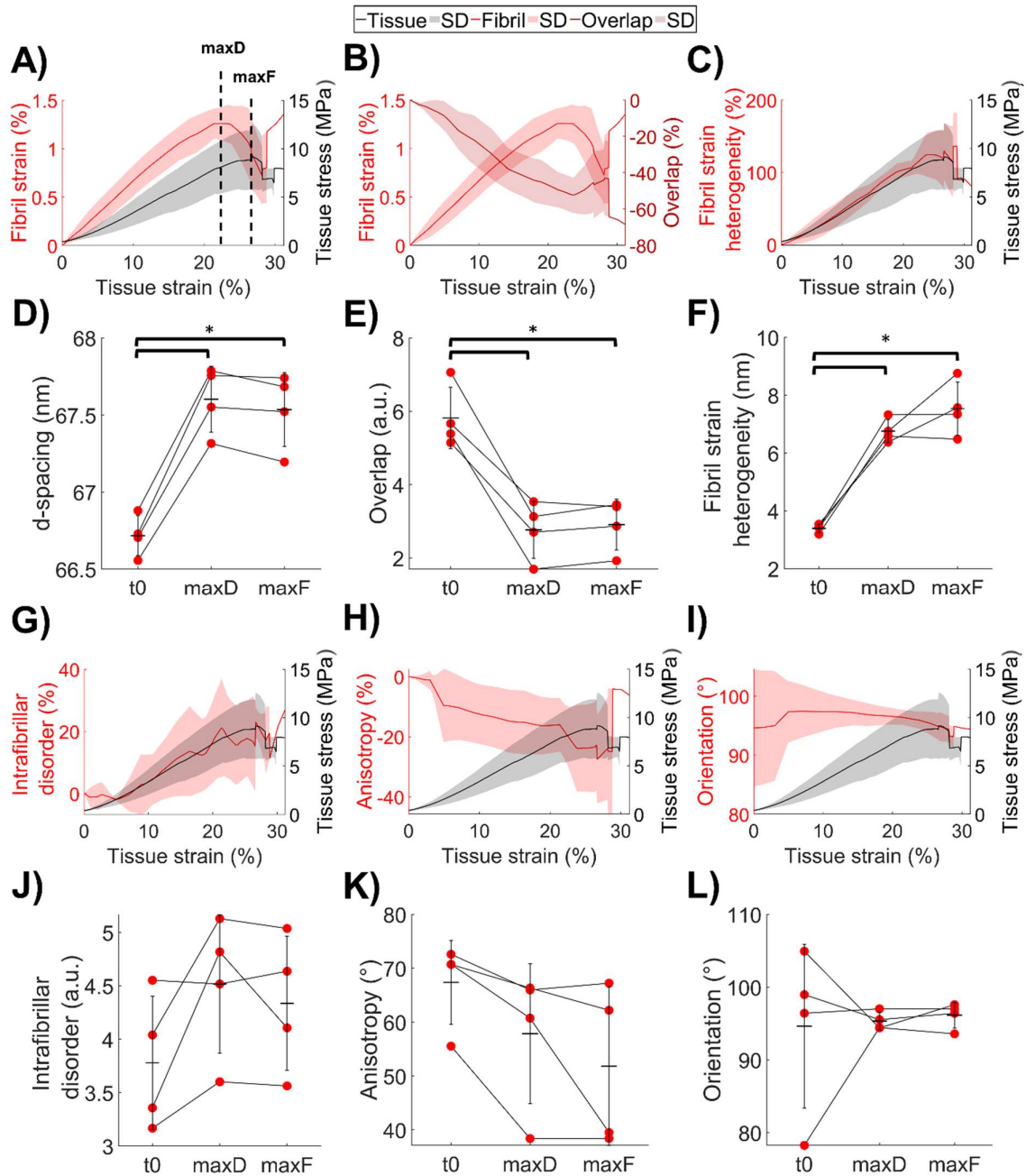
147 During *in situ* SAXS with simultaneous tensile loading in a ramp to failure configuration,
 148 macroscopic failure occurred at tissue stresses of 9.1 ± 2.3 MPa and strains of $27 \pm 1.7\%$. The
 149 elastic modulus within the linear region was 45 ± 10 MPa. Within the elastic region, the fibril
 150 strain increased linearly with tissue strain (Figure 3.A). The fibrils within the probed volume
 151 showed a decrease in slope close to global tissue yield (Supporting information, figure S.1) and
 152 then fibril strains rapidly decreased after reaching maximum fibril strains of 1.3 ± 0.1 %.
 153 Generally, increased loading resulted in a decrease in the length of the overlap region (Figure

154 3.B,E). Further, the fibril strain heterogeneity increased with the applied load (Figure 3.C,F).
 155 The intrafibrillar disorder showed a slight initial decrease within the toe region ($-4.8 \pm 2.4 \%$)
 156 (Figure 3.G), which then increased as loading continued. Increased loading was also
 157 accompanied by a small increase in alignment of the collagen fibrils (i.e., a decrease in
 158 anisotropy, Figure 3.H,K) and a slight reorientation of the fibrils towards the direction of the
 159 applied load (90°) (Figure 3.I,L). The responses of each individual sample can be found in the
 160 Supporting information, figure S.2. The physiological implications of the observed fibril
 161 responses are summarized in Table 1.

162 **Table 1. Observed fibril responses during ramp to failure and their physiological implications.** Arrows
 163 indicate increase (\uparrow) or decrease (\downarrow) and (*) indicate statistical significance.

Collagen structural parameter	Physiological implication
d-spacing / fibril strain \uparrow	Collagen fibrils stretching (*)
Length of the overlap region \downarrow	Collagen molecules sliding relative each other (*)
Fibril strain heterogeneity \uparrow	Wider range of fibrils carrying different loads (*)
Intrafibrillar disorder \uparrow	Loss of crystallinity / regular arrangement
Anisotropy \downarrow Standard deviation of orientation \downarrow	Collagen fibrils aligning

164



165

166 **Figure 3. Fibril response during ramp to failure.** A-C and G-I) Collagen fibril structural responses during *in*
 167 *situ* loading. Data is shown as mean (solid line) and standard deviation (shaded area). The tissue stress is shown
 168 in black, whereas fibril parameters are shown in red. D-F and J-L) Comparison between absolute values of collagen
 169 fibril structural parameters at the start of loading (t0), point of maximum d-spacing (maxD) and maximum tissue
 170 force (maxF). Error bars represent 95% confidence interval and statistical difference based on Kruskal Wallis test
 171 is indicated by *.

172

173

174

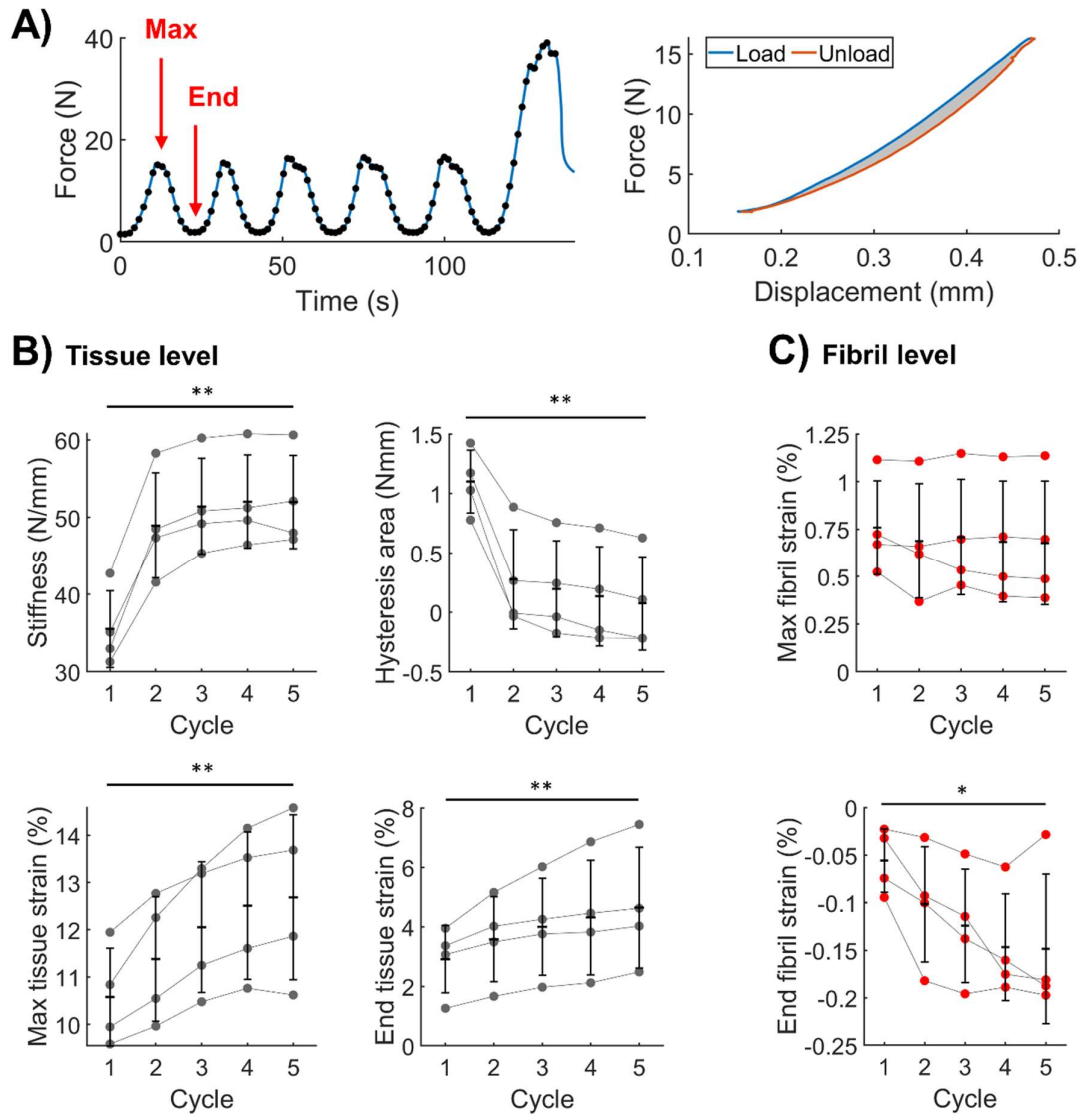
175 **3.3 Cyclic loading**

176 During *in situ* SAXS with simultaneous tensile loading in a cyclic configuration, increasing
 177 number of load cycles resulted in an increase in tissue stiffness and decrease in tissue hysteresis
 178 (Figure 4.B). Both maximum and end tissue strains also increased following number of applied
 179 load cycles. The maximum d-spacing and fibril strain measured during each load cycle
 180 remained similar (66.9 ± 0.4 nm, 0.7 ± 0.3 %). Further, the fibril strain during each load cycle
 181 was kept within the elastic region and never exceeded the failure strain observed during ramp
 182 to failure (Figure 3.A). Contrariwise, the d-spacing and strain at the end of each cycle slightly
 183 decreased with increasing number of cycles, with d-spacing values that were up to 0.2% lower
 184 than the initial d-spacing at the start of loading (Figure 4.C). All other parameters regained their
 185 starting values following unloading at each cycle. The collagen fibril strain, length of overlap
 186 region, and heterogeneity of the fibril strain distribution adapted and responded to the applied
 187 load in a similar manner as during ramp to failure (Figure 5.A-C). However, the response in
 188 intrafibrillar disorder and fibril alignment varied largely between specimens (Figure 5.D-E).
 189 The physiological implications of the observed fibril responses are summarized in Table 2.

190 **Table 2. Observed fibril responses during cyclic loading and their physiological implications.** Dash (-)
 191 indicates no change, arrows indicate increase (↑) or decrease (↓) and (*) indicate statistical significance.

Collagen structural parameter	Physiological implication
Maximum d-spacing / fibril strain -	Collagen fibrils stretching to similar values
End d-spacing / fibril strain ↓	Collagen fibrils relaxing (*)
Length of the overlap region ↓↑	Collagen molecules sliding apart and then back
Fibril strain heterogeneity ↑↓	Fibril load distribution increases and then decreases

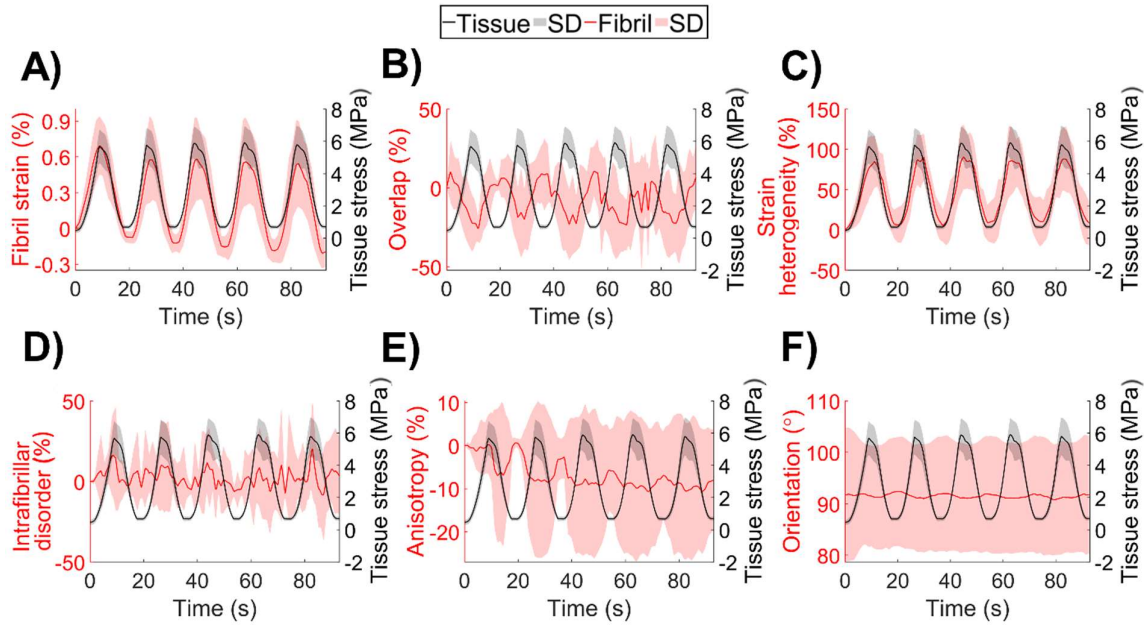
192



193

194 **Figure 4. Changes in tissue and fibril parameters during cyclic loading** A) Representative force vs time curve,
 195 indicating the maximum and final values of each cycle, and representative hysteresis curve, indicating the
 196 hysteresis area (grey) between the load and unload curves. B) Evolution of tissue level parameters with load cycles.
 197 C) Evolution of maximum and final fibril strain at each load cycle. The values corresponding to each individual
 198 specimen are indicated with lines. Error bars represent the 95% confidence interval and the statistical significance
 199 across all load cycles based on Friedmans test is indicated as ** $p < 0.01$ and * $p < 0.05$.

200



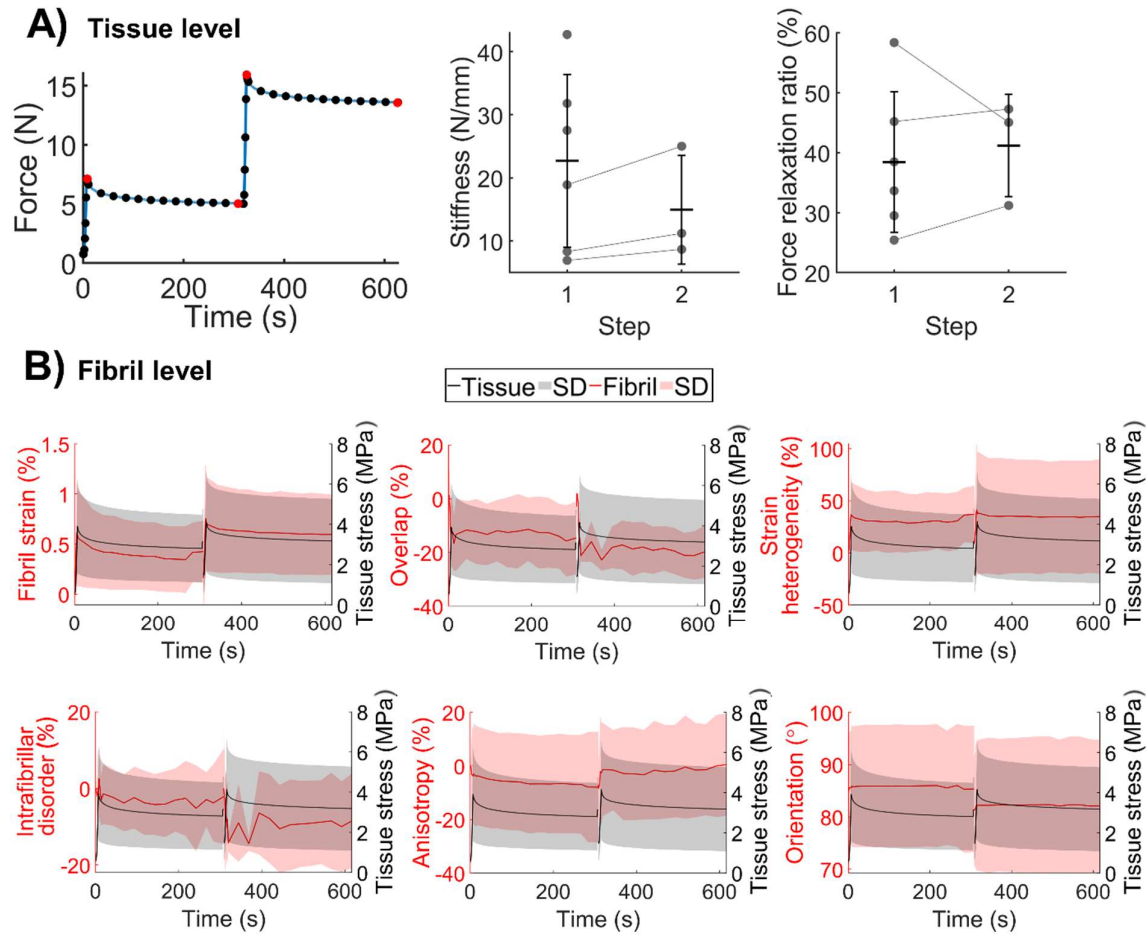
201

202 **Figure 5. Fibril behavior compared to applied force during cyclic loading.** A) Fibril strain, B) length of the
 203 overlap region, C) fibril strain heterogeneity, D) interfibrillar disorder, E) fibril anisotropy, and F) fibril main
 204 orientation. Data is shown as mean (solid line) and standard deviation (shaded area). The parameter from tissue
 205 level (force) is shown in black, whereas fibril parameters are shown in red.

206

207 3.3 Stress relaxation

208 During *in situ* SAXS with simultaneous tensile loading in a stress relaxation configuration,
 209 the 0.3 mm displacement steps equated to strain steps of 6.4 ± 0.4 %. Three specimens failed
 210 already during the second displacement step and are thus only included in the first step. In the
 211 remaining specimens, the stiffness and the force-relaxation ratio increased slightly between the
 212 first and the second steps (Figure 6.A). During tissue relaxation, relaxation of the fibrils was
 213 also observed (Figure 6.B, Fibril strain). However, the other fibril parameters did not show any
 214 clear relaxation trends.



215

216 **Figure 6. Tissue and fibril behavior during stress relaxation.** A) Tissue level behavior, showing a representative
 217 force time curve, indicating the maximum force and final values of each step (red dots) used for estimating stress
 218 relaxation ratios, as well as stiffness and stress relaxation ratios of each step. The values corresponding to each
 219 individual specimen are indicated with lines and error bars represent the 95% confidence interval B) Fibril
 220 level behavior during tissue relaxation. Data is shown as mean (solid line) and standard deviation (shaded area). The
 221 parameter from tissue level (force) is shown in black, whereas fibril parameters are shown in red.

222

223 4 DISCUSSION

224 This study combined SAXS with simultaneous *in situ* loading of whole rat Achilles tendons,
 225 to characterize the mechanical response of the collagen nanostructure in relation to the tissue
 226 scale response. The results show a clear simultaneous adaptation of the collagen structure to the
 227 applied tissue loads. Further, the combined results from the different loading scenarios indicate
 228 the extension of elastic and viscoelastic properties of the Achilles tendon down to the nanoscale.

229 From the radiation damage tests it was found that during the ramp to failure tests (0.75-0.95
230 s of beam exposure), the d-spacing reduced with approximately 0.05%, which was only
231 approximately 4% of the total fibril strain due to loading. During the stress relaxation (2.2 s of
232 beam exposure) and cyclic loading (3.5-4.6 s of beam exposure) tests, the d-spacing reduced
233 with approximately 0.1% and 0.2-0.3% respectively, which both accounted to approximately
234 20% of the total fibril strains due to loading. This indicates that the findings from this study
235 were not severely influenced by radiation damage.

236 **4.1 Loading affects intrafibrillar disorder in a bimodal manner**

237 By measuring the area under the collagen peaks to estimate the intrafibrillar disorder, this
238 study accounts for fibril strain heterogeneities and size of the coherently diffracting domains.
239 The axial intrafibrillar disorder decreased within the toe region, but then increased as loading
240 continued. This loss of intrafibrillar order could be due to the interface between the gap and
241 overlap zones becoming less well defined ^[14]. Only a few studies on rat tail tendons ^[14,20] and
242 cartilage ^[32] have previously reported the evolution of intrafibrillar order during *in situ* loading.
243 Even though the studies on tail tendons estimated the intrafibrillar order from the peak intensity,
244 their results are in line with this study. Misof et al. (1997) ^[20] observed that the lateral
245 intrafibrillar order increased within the toe region and Fratzl et al. (1997) ^[14] observed a
246 decrease of axial intrafibrillar order as the tendon is stretched into and beyond the “quasi-linear”
247 strain range, possibly due to internal structural breakdown occurring within the fibrils.
248 Additionally, Inamdar et al. ^[32] observed an increase in intrafibrillar disorder with decreasing
249 d-spacing during compression, which is parallel to the trends seen in tendons.

250 **4.2 Collagen peak width is related to strain heterogeneity**

251 In the current study, the fibril strain heterogeneity started to increase at low loads and kept
252 on increasing continuously throughout loading. This contradicts the findings in a study by

253 Fessel et al. (2014) ^[9], where the fibril strain heterogeneity in rat tail tendons remained constant
254 up until tissue yield and then suddenly increased. This discrepancy could be due to using a
255 different displacement rate (~2.4 times faster in Fessel et al.) or the assumption that the
256 broadening of the collagen peak is solely related to strain heterogeneity in rat tail tendons. The
257 change in peak width could arise from two phenomena: strain and changes in the size of
258 coherently diffracting domains ^[33]. To our knowledge, no study has evaluated what mechanism
259 the broadening of the collagen peaks is attributed to. The different contributions can be obtained
260 from a Williamson-Hall plot ^[34,35]. In the current study, following increased loading of the
261 Achilles tendons, the slope of this plot increased whereas the intersect with the y-axis remained
262 relatively constant (Supporting information, figure S.3). This confirms the assumption that the
263 increase in peak width during loading in this study indeed is related to strain heterogeneity and
264 not changes in the size of the coherently diffracting domains. Additionally, two other factors
265 support this relation: 1) during cyclic loading, the width recovered during unloading and 2)
266 during ramp to failure, the width recovered during unloading after tissue failure in most
267 specimens (data not shown). Well in line with these results, Inamdar et al. (2021) ^[36] also
268 observed a recovery of peak width during cyclic loading in cartilage. The sudden change in
269 peak width reported by Fessel et al. (2014) ^[9], however, could instead have arisen from a sudden
270 change in the size of the coherently diffracting domains. Additionally, non-uniform strains of
271 the Achilles tendon have been shown, both in terms of the sub-tendons deforming differently
272 ^[37,38] as well as deformation differences between the deep and superficial layers of the tendon
273 ^[39,40].

274 **4.3 Increased fibril strain recovery might not be due to damage**

275 At lower loads within the elastic region of the tissue, the fibrils showed viscoelastic
276 properties, such as increased fibril strain recovery and stretchability during cyclic loading. The
277 successive decrease in d-spacing at the end of each load cycle could be attributed to one or a

278 combination of four different factors: 1) mechanical damage to the fibrils, 2) radiation damage
279 to the fibrils, 3) water flowing out of the structures or 4) interfibrillar matrix relaxation. As the
280 fibril strains never exceeded the fibril yield strain, it is highly unlikely this would be due to
281 mechanical damage. If the fibrils were damaged in any way, they would most likely also have
282 had an increase in maximum fibril strain, since a loss in integrity of the structure would have
283 disrupted its ability to respond to loads. Moreover, the fibril strain distribution also returned to
284 their initial values, indicating that the size of the coherently diffracting domains was not altered.
285 Dehydration studies of tendons have demonstrated that the d-spacing decreases with decreased
286 humidity ^[41-43]. By evaluating the equatorial scattering peak ^[6,32,44] (wet state: $q \sim 1.3-1.8 \text{ nm}^{-1}$
287 ¹, dry state: $q \sim 1.1 \text{ nm}^{-1}$), it is possible to gain information about the intrafibrillar hydration
288 state, but this peak could not be properly resolved with the measured q-range of this study.
289 There are presently no studies investigating this in tendons during *in situ* loading, but Inamdar
290 et al. (2017) ^[32] observed little to no change in fluid flow at the intrafibrillar level during *in situ*
291 stress relaxation of cartilage. However, cartilage is in a state of relative dehydration compared
292 to tendons, but the observed trend could potentially be similar. Gupta et al. (2010) ^[11] observed
293 a double exponential fibril relaxation response in rat tail tendons, which they suggested was
294 due to relaxation within the interfibrillar matrix. Hence, we hypothesize that in this study the
295 major contributor to the observed decrease in d-spacing at the end of each load cycle was also
296 due to interfibrillar matrix relaxation.

297 **4.4 Tissue relaxation is accompanied by fibril relaxation**

298 Simultaneously as the tissue underwent relaxation, fibril relaxation was observed. This is
299 well in line with previous studies on rat tail tendons, where the fibril relaxation ratios have been
300 shown to increase with increased strain steps ^[8,9]. However, no such consistent increase in
301 relaxation ratio was found between strain steps in this study. This could be due to the limited

302 sample numbers that were tested at step 2. Further, it could be due to the larger strain steps
303 taken within the current study ^[8,9] or a too slow strain rate.

304 **4.5 Fibril mechanical behavior within the tissue differs from single fibril mechanics**

305 Using SAXS to evaluate fibril strains in combination with *in situ* loading of whole tendons,
306 we and others ^[8-10,15,22] have observed fibril strains substantially lower than those from
307 dissected single fibrils ^[16-19] (fibril failure strains ~1.3-4% vs 11-27 %). However, Svensson et
308 al. ^[18] observed that the fibril strain recorded at the ends (13-14 % for fibrils from Achilles
309 tendons) was increased compared to central strains as measured by optical tracking of the same
310 fibrils (8.5-8.9 %), which could indicate that the strains reported in single fibril studies are
311 slightly over-estimated. Quigley et al. ^[19] and Svensson et al. ^[16] showed that fibrils from energy
312 storing tendons exhibit a three-phase behavior instead of the two-phased behavior observed in
313 fibrils from positional tendons. This three-phase behavior of the collagen fibrils was not
314 observed in this study, nor in the previous studies combining *in situ* loading with synchrotron
315 SAXS on rat tail tendons, where the fibrils instead exhibited a linear increase in strain until they
316 came to an abrupt decrease close to tissue yield or failure ^[8,9,22].

317 The higher fibril strains observed in single fibril studies demonstrate the capability of collagen
318 fibrils to extend further than they do when inside the tendon. Studies based on different
319 microscopical techniques at several parts of the tissue ^[45-48], indicate fibril continuity along the
320 entire tendon. In this case, the fibril response in the full tissue should be similar to that of the
321 single fibril. However, studies based on mechanical testing in combination with X-ray
322 diffraction, confocal, and atomic force microscopy strongly suggest that strain is being
323 partitioned between the fibrils and the fibers. The strain then occurs through interfibrillar and
324 interfiber shear forces, and thus that the fibrils instead are functionally discontinuous <sup>[11,22,49-
325 53]</sup>. In this study, we found fibril elongation to be affected by two simultaneous mechanisms:
326 stretching and sliding. Even though sliding was observed already at the beginning of loading,

327 it was not as prominent during small strains as during larger strains. This is well in line with
328 similar studies on rat tail tendons [9,13,54] and this presence of fibril sliding further supports
329 functional discontinuity of fibrils in the tendon. Instead, there is probably a complex coupling
330 between different hierarchical levels, which contribute to the strain being partitioned and the
331 single fibril thus not carrying the entire applied load. The fact that the fibrils do not reach as
332 high strains while in this intricate arrangement could also explain why the fibrils do not reach
333 the other phases observed in single fibrils by Quigley et al. [19] and Svensson et al. [16] .
334 Additionally, this points towards macroscopic tissue damage and failure not being initiated
335 within the fibrils, but rather in the structures between fibrils, fibers and sub-tendons, as implied
336 by previous studies on fibril and fiber mechanics within full tendons or fascicles [11,22,49–51].

337 **4.6 Comparison of energy-storing tendons and positional tendons**

338 All of the Achilles tendons evaluated in this study had a slightly smaller d-spacing prior to
339 loading (66.6 nm) as well as slightly lower fibril failure strains (1.3 %) compared to fascicles
340 from rat tail tendons evaluated using the same techniques and approach (67.5-67.7 nm, 1.5-4
341 %) [8–10,22]. Quigley et al. [19] showed that single fibrils from positional and energy-storing
342 tendons not only exhibited different mechanical responses, but those from energy-storing
343 tendons were also stronger, had a higher elastic modulus and did not form kinks nor a reduction
344 in shell delamination in response to rupture. In line with this, Svensson et al. [18] showed that
345 fibrils from Achilles tendons strained slightly less than those from rat tail tendons. These
346 differences could be one reason behind the d-spacing and fibril strains observed in this study
347 being within the lower range of similar studies on rat tail tendons.

348 In this study, the fibrils themselves seem to exhibit plastic damage, indicated by their response
349 shortly before failure being nonlinear (Supporting information, figure S.1), which in turn
350 suggest the presence of intrafibrillar damage prior to fibril failure. The fact that the fibrils show
351 an nonlinear response prior to fibril failure contradicts similar studies on rat tail tendons where

352 the fibril failure was found to be abrupt and the equatorial SAXS reflections to completely
353 disappear following tissue yield ^[8,9]. In this study however, whilst at a much lower intensity,
354 the reflections remain and the d-spacing continues to change.

355 Neither the earlier studies on rat tail tendons ^[8-10,22] nor a lab-based study on explants from
356 bovine Achilles tendons ^[54] related the findings to the whole tissue level, thus not considering
357 the interplay between all hierarchical levels of the tissue. By not testing the full tissue, the strain
358 will most likely not be partitioned as in its native state. Thus, the fibrils could potentially
359 experience higher loads, resulting in higher strains. Thorpe et al. (2012, 2015) ^[25,27] recently
360 highlighted the major contribution of the interfascicular matrix to the overall mechanical
361 properties. Their finding and the slight discrepancies in fibril strain levels and behavior between
362 the current study and previous studies on rat tail tendons further emphasizes the need for
363 studying more than one hierarchical level of the tissue at a time as well as the need for more
364 studies on energy-storing tendons.

365 The discrepancies between rat tail fascicles and Achilles tendons together with the overall
366 results of this study further highlights the heterogenous and complex response a tendon exhibit
367 across several length scales, and this needs to be taken more often into account in mechanical
368 studies. Future studies aimed at characterizing the mechanical response of tendons should
369 therefore apply suitable techniques to resolve the inner mechanical heterogeneity of the tendon
370 during loading, using e.g. SAXS or phase-contrast tomography for fibril and fiber levels
371 respectively. Although, as this study focuses on the relation between macroscopic and
372 nanoscale behaviors, a simplified assumption was still made for tissue scale stresses and strains.

373 **4.7 Limitations**

374 Compared to the physiological loading rate of tendons, the displacement rate in this study
375 was low. Therefore, there is an uncertainty in separation between the fibril elastic response,
376 sliding, and relaxation. Thus, more studies using a higher displacement rate need to be

377 conducted to confirm the fibril strain values in this study. Additionally, no preconditioning was
378 performed prior to the mechanical tests, which most likely contributes to the large inter-sample
379 variabilities in especially the cyclic loading and stress relaxation tests. Nevertheless, all samples
380 followed similar trends in their fibril responses. Moreover, the clamping of the tendons in this
381 loading device could be improved as the tendons were often observed to break close to the
382 clamps, which is most likely one reason behind the tissue failure strains and stresses of this
383 study being relatively high and low, respectively. However, that is a common problem when
384 performing mechanical testing of intact Achilles tendons. Additionally, the setup did not allow
385 the tests to be conducted in a bath, but for the short measurement times in this experiment, the
386 Kapton film was sufficient to keep the tendons hydrated throughout the tests. Lastly, the
387 scattering data were acquired from a limited volume ($\sim 1 \times 0.15 \times 0.15 \text{ mm}^3$) in the center of the
388 tendon and is thus averaged over many collagen fibrils in the path of the beam. Therefore, the
389 measurements most likely do not include regional differences within the tendon, as was further
390 confirmed with narrow, normally distributed angular intensities. In some samples however, the
391 distribution contained a small shoulder, indicating a slight heterogeneity within the fibril
392 population. This could be interpreted as more than one sub-tendon being present within the
393 beam path in these cases.

394

395 **5 CONCLUSIONS**

396 The powerful combination of *in situ* loading during synchrotron SAXS acquisitions enabled
397 characterization of the relationship between the tissue and nanoscale responses in energy-
398 storing rat Achilles tendons for both elastic and viscoelastic loading scenarios. In this study, the
399 mechanical and functional effects of the complex hierarchical structure of the Achilles tendon
400 were evaluated. The results show substantially lower fibril strain than the applied tissue strain
401 and thus further support strain partitioning between hierarchical levels. Additionally, it was

402 shown that both elastic and viscoelastic properties are transferred down to the fibril level. This
403 study provides further insight into the non-uniform deformation mechanisms of the Achilles
404 tendon by determining that fibril strain heterogeneity is related to changes in collagen peak
405 width. All together, these results stress the importance and need for future studies to thoroughly
406 consider heterogeneity when evaluating the mechanical behavior of tendons. Our approach
407 provides the unique possibility of studying the nanostructural response of collagen fibrils within
408 the complex arrangement of the tendon. These results could represent the basis for future studies
409 of different pathologies or injuries affecting tendons, as well as pave the way for similar studies
410 of other collagen-based tissues.

411

412 **2 METHODS**

413 **2.1 Samples**

414 Female specific pathogen free (SPF) Sprague Dawley rats (N = 15), aged 10-14 weeks
415 (weight 219 ± 21 g), were used (Janvier, Le Genest-Saint-Isle, France). The rats were kept two
416 per cage under controlled humidity (55 %) and temperature (22 °C), with a light-dark cycle of
417 12 hours. They were given standard food pellets and water *ad libitum*. After euthanization with
418 carbon dioxide, the plantaris tendon was removed and the Achilles tendon was harvested
419 together with the calcaneal bone and the gastrocnemius soleus muscle complex. The tendons
420 were wrapped in gauze soaked in phosphate buffered saline (PBS) solution and stored frozen (-
421 20 °C) until measurements (approximately 3 months). The storage does not affect the tissue
422 mechanics ^[55,56], but may cause an increased water content. The experiment adhered to the
423 institutional guidelines for care and treatment of laboratory animals and was approved by the
424 Regional Ethics Committee for animal experiments in Linköping, Sweden (ID1424).

425

426 2.2 Synchrotron small-angle X-ray scattering and *in situ* loading

427 SAXS measurements were carried out at the coherent small-angle X-ray scattering beamline
428 (cSAXS) at the Swiss Light Source (SLS), Paul Scherrer Institut (PSI), Switzerland. The
429 samples were thawed, and sagittal and transverse diameters were measured with a slide caliper
430 at the middle of the tendon. The cross-sectional area was calculated assuming an elliptical
431 geometry. Kapton film (8 μm , 3512, SPEX Sample Prep, USA) was placed around each tendon
432 and held together with a drop of PBS, to keep the tendon hydrated during the experiments
433 (Figure 1.A). The specimens were mechanically loaded at the beamline using a custom-built
434 tensile test device designed for *in situ* measurements, similar to earlier studies [57,58]. The device
435 was mounted on two linear stages along the two directions perpendicular to the beam path and
436 controlled using a custom-made control software in LabVIEW (National Instruments Corp.,
437 US). During the experiment, the device was run in displacement control mode. The load was
438 measured with a 111 N (25 lbf) load cell with an accuracy of $\pm 1\%$ (LC201 25, Omega
439 Engineering Inc., USA). To minimize slipping, sandpaper was placed on the muscle bundle
440 before clamping in the ribbed upper grip of the loading device, making sure that the clamps
441 were placed below the site of visible fascicle branching. The distal end was clamped just above
442 the calcaneal bone. Due to the design of the grips, the tendons were mounted straight, simulating
443 extreme plantarflexion. Using a camera mounted at the beamline, a picture before and after the
444 tests were acquired for visual evaluation of potential slippage.

445 The tendons were loaded in tension by equally displacing both grips simultaneously with a
446 rate of 5 mm/min ($1.8 \pm 0.3\%$ L0/s), keeping the center of the tendon in the path of the beam
447 and thus the measured region constant throughout the test. A force transducer measured the
448 axial force and a linear displacement sensor recorded the displacement of the grips. All tendons
449 were preloaded to 1 N before each loading scheme was applied. To preserve tendon hydration,
450 no additional precondition was performed as this would have substantially prolonged the

451 duration of the tendon being inside the experimental hutch due to limitations in the control
452 software implementation. Three loading schemes were applied (Figure 1.B):

- 453 1) ramp to failure ($N = 5$), where the tendons were stretched until tissue failure,
- 454 2) cyclic loading ($N = 4$), where 5 cycles of 2-15 N were performed,
- 455 3) stress relaxation ($N = 6$), where the tendons were displaced in 0.3 mm steps, followed
456 by 300 s relaxation per step for 2 consecutive steps.

457 The magnitudes of cyclic force and displacement steps were chosen to be within the elastic
458 region based on tests with the loading device prior to the experiment.

459 SAXS acquisitions were conducted at intervals of 1.2 s during ramp to failure and cyclic
460 loading. During stress relaxation, 10 SAXS acquisitions were conducted at intervals of 1.2 s
461 during the initial loading phase and early relaxation, followed by 12 SAXS acquisitions
462 conducted at intervals of 25 s during the remaining of the relaxation phase (Figure 1.B).

463 SAXS measurements were conducted using a beam energy of 12.4 keV (wavelength of ~ 1
464 \AA) and a sample-detector distance of 7.146 m, enabling data acquisition in the q -range of 0.02-
465 1.45 nm^{-1} . The sample-detector distance and beam center were determined using a silver
466 behenate powder standard. An off-axis optical microscope calibrated with the X-ray beam
467 position was used to find the center of the tendon, where SAXS acquisition was conducted
468 using a beam size of $150 \times 125 \text{ }\mu\text{m}^2$ (horizontal \times vertical) and an exposure time of 50 ms. The
469 beam flux was measured (3.0×10^{11} photons/s) using a glassy carbon standard specimen ^[59]. The
470 2D scattering patterns were recorded with a Pilatus 2M detector ($1475 \times 1679 \text{ pixels}^2$, pixel size
471 $172 \times 172 \text{ }\mu\text{m}^2$). Measurements of only the Kapton film next to the samples were conducted for
472 background correction. To investigate the effects of the dose rate on the specimens, this beam
473 configuration was compared to a second configuration with higher number of incident X-rays
474 onto the measured sample area, by reducing the beam size to $32 \times 20 \text{ }\mu\text{m}^2$ and thus providing a
475 measured flux of approximately 1.7×10^{11} photons/s.

476 2.3 Data analysis

477 Analysis of the 2D scattering patterns was performed using in-house codes in Matlab®
478 (R2019a, MathWorks Inc, USA) as previously described by Turunen et al. (2017) [60]. The
479 beam stop was masked away from the scattering patterns, along with dead or over-exposed
480 pixels and gaps between detector modules. To obtain the $I(\theta)$ curves, the scattering patterns
481 were angularly integrated over 0-360° in the q -regions of the 3rd-10th meridional reflections
482 (indicated by non-shaded areas in Figure 1.C). The $I(\theta)$ peaks were fitted with Gaussian curves
483 and the predominant orientation of the collagen fibrils was determined from the position of the
484 fit (Figure 6.C). The degree of anisotropy, i.e. the dispersion in fibril orientation, was
485 determined as the full-width-at-tenth of maximum (FWTM) of this fit [60,61]. The $I(q)$ scattering
486 curves were obtained in the q -region of 0.05-1.45 nm⁻¹ by radially integrating the scattering
487 patterns over the main fibril orientation $\pm 60^\circ$ to cover the meridional scattering (indicated by
488 non-shaded areas in Figure 1.D), giving rise to peaks related to each meridional collagen
489 reflection (blue curve in Figure 1.D). Gaussian curves were fitted to the 1st through 10th collagen
490 peaks of the $I(q)$ curve. The 3rd peak was used to determine the collagen periodicity (d-spacing)
491 as the peak position and the fibril strain heterogeneity, i.e. dispersion in fibril strains, as changes
492 in full-width-at-half-maximum (FWHM). The intensity ratio between the 3rd and 2nd peaks
493 (I_3/I_2) was calculated from their respective peak areas and used to estimate changes in the length
494 of the overlap region (O), which varies when adjacent collagen molecules slide relative to each
495 other [43,54]. The relationship between relative intensity of collagen peaks of order m and n can
496 be described by [9,10,54,60]:

$$497 \quad \frac{I_m}{I_n} = \left(\frac{n}{m}\right)^2 \left[\frac{\sin(m\pi O/d)}{\sin(n\pi O/d)}\right]^2 \quad (1)$$

498 where I_n and I_m are the intensity of the n^{th} and m^{th} order collagen peaks respectively, O is the
499 overlap length, and d is the d-spacing.

500 When a degree of disordering of the gap/overlap interface is present, the intensity of higher
 501 order peaks is reduced by a larger amount compared to lower order peaks [14,32]. This reduction
 502 can be described by applying a Debye-Waller type factor $\exp(-\kappa q^2)$, where κ is proportional
 503 to the disordering and $q_n = \frac{2\pi n}{D}$, to equation 1 [32]:

$$504 \quad \frac{I_m}{I_n} = \left(\frac{n}{m}\right)^2 \left[\frac{\sin(m\pi O/d)}{\sin(n\pi O/d)}\right]^2 \exp\left(-\kappa(m^2 - n^2)\left(\frac{2\pi}{D}\right)^2\right) \quad (2)$$

505 The intensity ratio between the 5th and 7th order collagen peaks (I_5/I_7) was calculated from their
 506 respective peak areas and used to estimate changes in intrafibrillar disorder, which increases
 507 when the interface between gap and overlap region gets less distinct [14,32].

508 The force applied to the tissue was normalized to the cross-sectional area of the tendon (2.3
 509 $\pm 0.7 \text{ mm}^2$) to obtain tissue stress (σ). Tissue strain (ε_T) and fibril strain (ε_F) were obtained by
 510 normalizing the tissue displacement and collagen d-spacing to their starting values [9]:

$$511 \quad \varepsilon_T = (L - L_0)/L_0 \quad (3)$$

$$512 \quad \varepsilon_F = (d - d_0)/d_0 \quad (4)$$

513 where L is the displaced tissue length, L_0 the initial distance between the grips at preload (4.6
 514 $\pm 0.7 \text{ mm}$), d the d-spacing, and d_0 the initial d-spacing at preload ($66.6 \pm 0.2 \text{ nm}$). Stiffness
 515 was determined from a fit of the linear region in the load curve and the yield point was estimated
 516 as 0.2 % strain offset from this fit (post-linear region). Hysteresis was determined per cycle as
 517 the area between the loading and unloading force-displacement curve. Stress relaxation ratio
 518 corresponded to the relative decrease in force from the start of each step until the end of the
 519 relaxation period.

520 **2.4 Radiation damage**

521 Radiation dose is an important and limiting factor when studying biological samples such as
 522 tendons, as too high doses can damage the tissues and especially affect their mechanical
 523 properties [62]. Thus, prior to mechanical testing, a radiation damage test was conducted on a

524 tendon not subjected to mechanical load to ensure that the repeated SAXS exposure would not
525 significantly affect the collagen structure. Two dose rates were compared by varying the beam
526 size ($150 \times 125 \mu\text{m}^2$ or $32 \times 20 \mu\text{m}^2$) and repeatedly acquiring SAXS measurements at one spot.
527 The sample transmission was estimated from the number of photons recorded at the beam stop
528 with and without a sample in the beam path. The absorption ratio was calculated from the
529 recorded transmission at the beam stop, as the ratio of photons not being transmitted. The tissue
530 density was estimated to be between $1050\text{-}1120 \text{ kg/m}^3$, based on typical values reported for soft
531 tissues such as muscle, cartilage, skin and tendons ^[63,64]. The total dose (D) deposited on the
532 sample was defined as the energy absorbed by the sample divided by the sample mass, and was
533 calculated as:

534
$$D = \frac{I_0 \cdot \tau \cdot A \cdot E}{\Delta_x \Delta_y \Delta_z \cdot \rho} \quad (5)$$

535 where I_0 is the photon flux (photons/s), τ is the exposure time, A is the absorption ratio, E the
536 X-ray energy, $\Delta_x \Delta_y \Delta_z$ is the scattering volume (beam area \times sample thickness), and ρ the mass
537 density of the sample.

538 2.5 Statistics

539 Mean, standard deviation (SD) and 95% confidence intervals (CI) were calculated. Non-
540 parametric tests were selected as the number of samples was too small to ensure normally
541 distributed data. In ramp to failure, the Kruskal-Wallis test was used to test for statistical
542 difference between start of loading (t_0), maximum d-spacing (maxD) and maximum force
543 (maxF) (R2019a, MathWorks Inc., USA). In cyclic loading, the Friedman's test was used to
544 test for statistical differences across multiple load cycles.

545

546 ACKNOWLEDGEMENTS

547 This project has received funding from the Knut and Alice Wallenberg Foundation
548 (WAF2017) and the European Research Council (ERC) under the European Union’s Horizon
549 2020 research and innovation programme (grant agreement No 101002516). We acknowledge
550 the European Union’s Horizon 2020 research and innovation programme under grant agreement
551 No 731019 (EUSMI), which provided beamtime at the cSAXS beamline, Paul Scherrer Institut,
552 Switzerland, as well as the Paul Scherrer Institut and the beamline staff at cSAXS for help
553 before, during and after the beamtime.

554

555 REFERENCES

- 556 1. Fratzl P. Cellulose and collagen: From fibres to tissues. Vol. 8, Current Opinion in
557 Colloid and Interface Science. Elsevier BV; 2003. p. 32–9.
- 558 2. Fratzl P, Weinkamer R. Nature’s hierarchical materials. Prog Mater Sci.
559 2007;52(8):1263–334.
- 560 3. Veis A. Collagen fibrillar structure in mineralized and nonmineralized tissues. Curr Opin
561 Solid State Mater Sci. 1997;2(3):370–8.
- 562 4. Petruska JA, Hodge AJ. A subunit model for the tropocollagen macromolecule. Proc
563 Natl Acad Sci United States. 1964;51:871–6.
- 564 5. Orgel JPRO, Irving TC, Miller A, Wess TJ. Microfibrillar structure of type I collagen in
565 situ. Proc Natl Acad Sci U S A. 2006;103(24):9001–5.
- 566 6. Fratzl P, Fratzl-Zelman N, Klaushofer K. Collagen packing and mineralization. An x-
567 ray scattering investigation of turkey leg tendon. Biophys J. 1993;64(1):260–6.
- 568 7. Gupta HS. Chapter 7: Nanoscale Deformation Mechanisms in Collagen. In: Fratzl P,
569 editor. Collagen: Structure and Mechanics, an introduction. Boston: Springer US; 2008.
- 570 8. Gautieri A, Passini FS, Silván U, Guizar-Sicairos M, Carimati G, Volpi P, Moretti M,
571 Schoenhuber H, Redaelli A, Berli M, et al. Advanced glycation end-products: Mechanics
572 of aged collagen from molecule to tissue. Matrix Biol. 2017;59:95–108.
- 573 9. Fessel G, Li Y, Diederich V, Guizar-Sicairos M, Schneider P, Sell DR, Monnier VM,
574 Snedeker JG. Advanced glycation end-products reduce collagen molecular sliding to
575 affect collagen fibril damage mechanisms but not stiffness. PLoS One. 2014;9(11).
- 576 10. Bianchi F, Hofmann F, Smith AJ, Thompson MS. Probing multi-scale mechanical
577 damage in connective tissues using X-ray diffraction. Acta Biomater. 2016 Nov
578 1;45:321–7.
- 579 11. Gupta HS, Seto J, Krauss S, Boesecke P, Screen HRC. In situ multi-level analysis of

- 580 viscoelastic deformation mechanisms in tendon collagen. *J Struct Biol.*
581 2010;169(2):183–91.
- 582 12. Szczesny SE, Fetchko KL, Dodge GR, Elliott DM. Evidence that interfibrillar load
583 transfer in tendon is supported by small diameter fibrils and not extrafibrillar tissue
584 components. *J Orthop Res.* 2017;35(10):2127–34.
- 585 13. Folkhard W, Mosler E, Geercken W, Knörzer E, Nemetschek-Gansler H, Nemetschek
586 T, Koch MHJ. Quantitative analysis of the molecular sliding mechanisms in native
587 tendon collagen - time-resolved dynamic studies using synchrotron radiation. *Int J Biol*
588 *Macromol.* 1987;9(3):169–75.
- 589 14. Fratzl P, Misof K, Zizak I, Rapp G, Amenitsch H, Bernstorff S. Fibrillar Structure and
590 Mechanical Properties of Collagen. *J Struct Biol.* 1997;122:119–22.
- 591 15. Knörzer E, Folkhard W, Geercken W, Boschert C, Koch MHJ, Hilbert B, Krahl H,
592 Mosler E, Nemetschek-Gansler H, Nemetschek T. New aspects of the etiology of tendon
593 rupture - An analysis of time-resolved dynamic-mechanical measurements using
594 synchrotron radiation. *Arch Orthop Trauma Surg.* 1986;105(2):113–20.
- 595 16. Svensson RB, Mulder H, Kovanen V, Magnusson SP. Fracture mechanics of collagen
596 fibrils: Influence of natural cross-links. *Biophys J.* 2013;104(11):2476–84.
- 597 17. Svensson RB, Eriksen CS, Tran PHT, Kjaer M, Magnusson SP. Mechanical properties
598 of human patellar tendon collagen fibrils. An exploratory study of aging and sex. *J Mech*
599 *Behav Biomed Mater.* 2021;124(April):104864.
- 600 18. Svensson RB, Smith ST, Moyer PJ, Magnusson SP. Effects of maturation and advanced
601 glycation on tensile mechanics of collagen fibrils from rat tail and Achilles tendons. *Acta*
602 *Biomater.* 2018;70:270–80.
- 603 19. Quigley AS, Bancelin S, Deska-Gauthier D, Légaré F, Kreplak L, Veres SP. In tendons,
604 differing physiological requirements lead to functionally distinct nanostructures. *Sci*
605 *Rep.* 2018;8(1).
- 606 20. Misof K, Rapp G, Fratzl P. A new molecular model for collagen elasticity based on
607 synchrotron x- ray scattering evidence. *Biophys J.* 1997;72(3):1376–81.
- 608 21. Mosler E, Folkhard W, Knörzer E, Nemetschek-Gansler H, Nemetschek T, Koch MHJ.
609 Stress-induced molecular rearrangement in tendon collagen. *J Mol Biol.* 1985 Apr
610 20;182(4):589–96.
- 611 22. Puxkandl R, Zizak I, Paris O, Keckes J, Tesch W, Bernstorff S, Purslow P, Fratzl P.
612 Viscoelastic properties of collagen: Synchrotron radiation investigations and structural
613 model. *Philos Trans R Soc B Biol Sci.* 2002;357(1418):191–7.
- 614 23. Screen HRC, Toorani S, Shelton JC. Microstructural stress relaxation mechanics in
615 functionally different tendons. *Med Eng Phys.* 2013;35(1):96–102.
- 616 24. Thorpe CT, Klemm C, Riley GP, Birch HL, Clegg PD, Screen HRC. Helical sub-
617 structures in energy-storing tendons provide a possible mechanism for efficient energy
618 storage and return. *Acta Biomater.* 2013;9(8):7948–56.

- 619 25. Thorpe CT, Godinho MSC, Riley GP, Birch HL, Clegg PD, Screen HRC. The
620 interfascicular matrix enables fascicle sliding and recovery in tendon, and behaves more
621 elastically in energy storing tendons. *J Mech Behav Biomed Mater.* 2015;52:85–94.
- 622 26. Thorpe CT, Birch HL, Clegg PD, Screen HRC. Tendon Physiology and Mechanical
623 Behavior: Structure-Function Relationships. *Tendon Regeneration: Understanding*
624 *Tissue Physiology and Development to Engineer Functional Substitutes.* Elsevier Inc.;
625 2015. 3–39 p.
- 626 27. Thorpe CT, Udeze CP, Birch HL, Clegg PD, Screen HRC. Specialization of tendon
627 mechanical properties results from interfascicular differences. *J R Soc Interface.*
628 2012;9(76):3108–17.
- 629 28. Herod TW, Chambers NC, Veres SP. Collagen fibrils in functionally distinct tendons
630 have differing structural responses to tendon rupture and fatigue loading. *Acta Biomater.*
631 2016;42:296–307.
- 632 29. Choi RK, Smith MM, Smith S, Little CB, Clarke EC. Functionally distinct tendons have
633 different biomechanical, biochemical and histological responses to in vitro unloading. *J*
634 *Biomech.* 2019;95.
- 635 30. Hess G. Achilles tendon ruptures. *Foot ankle Spec.* 2009;3(1):29–32.
- 636 31. Fernández M, Keyriläinen J, Serimaa R, - al, Fernández M, Keyriläinen J, Serimaa R,
637 Torkkeli M, Karjalainen-Lindsberg M, Tenhunen M, et al. Related content Human breast
638 cancer in vitro Small-angle x-ray scattering studies of human breast tissue samples. Vol.
639 47, *Phys. Med. Biol.* 47 577 INSTITUTE OF PHYSICS PUBLISHING PHYSICS IN
640 MEDICINE AND BIOLOGY *Phys. Med. Biol.* 2002.
- 641 32. Inamdar SR, Knight DP, Terrill NJ, Karunaratne A, Cacho-Nerin F, Knight MM, Gupta
642 HS. The Secret Life of Collagen: Temporal Changes in Nanoscale Fibrillar Pre-Strain
643 and Molecular Organization during Physiological Loading of Cartilage. *ACS Nano.*
644 2017;11(10):9728–37.
- 645 33. Stokes AR, Wilson AJC. The diffraction of x rays by distorted crystal aggregates - I.
646 *Proc Phys Soc.* 1944;56(3):174–81.
- 647 34. Williamson GK, Hall WH. X-ray line broadening from filed aluminium and wolfram.
648 *Acta Metall.* 1953;1(1):22–31.
- 649 35. Khorsand Zak A, Abd. Majid WH, Abrishami ME, Yousefi R. X-ray analysis of ZnO
650 nanoparticles by Williamson-Hall and size-strain plot methods. *Solid State Sci.*
651 2011;13(1):251–6.
- 652 36. Inamdar SR, Prévost S, Terrill NJ, Knight MM, Gupta HS. Reversible changes in the 3D
653 collagen fibril architecture during cyclic loading of healthy and degraded cartilage. *Acta*
654 *Biomater.* 2021 Dec 1;136:314–26.
- 655 37. Finni T, Bernabei M, Baan GC, Noort W, Tijs C, Maas H. Non-uniform displacement
656 and strain between the soleus and gastrocnemius subtendons of rat Achilles tendon.
657 *Scand J Med Sci Sport.* 2018;28(3):1009–17.
- 658 38. Maas H, Noort W, Baan GC, Finni T. Non-uniformity of displacement and strain within

- 659 the Achilles tendon is affected by joint angle configuration and differential muscle
660 loading. *J Biomech.* 2020;101:109634.
- 661 39. Slane LC, Thelen DG. Non-uniform displacements within the Achilles tendon observed
662 during passive and eccentric loading. *J Biomech.* 2014 Sep 22;47(12):2831–5.
- 663 40. Franz JR, Slane LC, Rasske K, Thelen DG. Non-uniform in vivo deformations of the
664 human Achilles tendon during walking. *Gait Posture.* 2015;41(1):192–7.
- 665 41. Masic A, Bertinetti L, Schuetz R, Chang SW, Metzger TH, Buehler MJ, Fratzl P.
666 Osmotic pressure induced tensile forces in tendon collagen. *Nat Commun.* 2015 Jan 22;6.
- 667 42. Wess TJ, Orgel JP. Changes in collagen structure: Drying, dehydrothermal treatment and
668 relation to long term deterioration. *Thermochim Acta.* 2000;365(1–2):119–28.
- 669 43. Bigi A, Fichera AM, Roveri N, Koch MHJ. Structural modifications of air-dried tendon
670 collagen on heating. *Int J Biol Macromol.* 1987;9(3):176–80.
- 671 44. Lees S. Considerations regarding the structure of the mammalian mineralized osteoid
672 from viewpoint of the generalized packing model. *Connect Tissue Res.* 1987;16(4):281–
673 303.
- 674 45. Provenzano PP, Vanderby R. Collagen fibril morphology and organization: Implications
675 for force transmission in ligament and tendon. *Matrix Biol.* 2006 Mar;25(2):71–84.
- 676 46. Svensson RB, Herchenhan A, Starborg T, Larsen M, Kadler KE, Qvortrup K,
677 Magnusson SP. Evidence of structurally continuous collagen fibrils in tendons. *Acta*
678 *Biomater.* 2017 Mar 1;50:293–301.
- 679 47. Hijazi KM, Singfield KL, Veres SP. Ultrastructural response of tendon to excessive level
680 or duration of tensile load supports that collagen fibrils are mechanically continuous. *J*
681 *Mech Behav Biomed Mater.* 2019;97:30–40.
- 682 48. Craig AS, Birtles MJ, Conway JF, Parry DAD. An estimate of the mean length of
683 collagen fibrils in rat tail-tendon as a function of age. *Connect Tissue Res.*
684 1989;19(1):51–62.
- 685 49. Szczesny SE, Elliott DM. Interfibrillar shear stress is the loading mechanism of collagen
686 fibrils in tendon. *Acta Biomater.* 2014;10(6):2582–90.
- 687 50. Lee AH, Szczesny SE, Santare MH, Elliott DM. Investigating mechanisms of tendon
688 damage by measuring multi-scale recovery following tensile loading. *Acta Biomater.*
689 2017;57:363–72.
- 690 51. Fang F, Lake SP. Experimental evaluation of multiscale tendon mechanics. Vol. 35,
691 *Journal of Orthopaedic Research.* 2017. p. 1353–65.
- 692 52. Peterson BE, Szczesny SE. Dependence of tendon multiscale mechanics on sample
693 gauge length is consistent with discontinuous collagen fibrils. *Acta Biomater.* 2020 Nov
694 1;117:302–9.
- 695 53. Szczesny SE, Caplan JL, Pedersen P, Elliott DM. Quantification of interfibrillar shear
696 stress in aligned soft collagenous tissues via notch tension testing. *Sci Rep.*

- 697 2015;5:14649.
- 698 54. Sasaki N, Odajima S. Elongation mechanism of collagen fibrils and force-strain relations
699 of tendon at each level of structural hierarchy. *J Biomech.* 1996;29(9):1131–6.
- 700 55. Quirk NP, Lopez De Padilla C, De La Vega RE, Coenen MJ, Tovar A, Evans CH, Müller
701 SA. Effects of freeze-thaw on the biomechanical and structural properties of the rat
702 Achilles tendon. *J Biomech.* 2018;81:52–7.
- 703 56. Dietrich-Zagonel F, Hammerman M, Bernhardsson M, Eliasson P. Effect of storage and
704 preconditioning of healing rat Achilles tendon on structural and mechanical properties.
705 *Sci Rep.* 2021;11(1):1–10.
- 706 57. Engqvist J, Hall SA, Wallin M, Ristinmaa M, Plivelic TS. Multi-scale Measurement of
707 (Amorphous) Polymer Deformation: Simultaneous X-ray Scattering, Digital Image
708 Correlation and In-situ Loading. *Exp Mech.* 2014;
- 709 58. Gustafsson A, Mathavan N, Turunen MJ, Engqvist J, Khayyeri H, Hall SA, Isaksson H.
710 Linking multiscale deformation to microstructure in cortical bone using in situ loading,
711 digital image correlation and synchrotron X-ray scattering. *Acta Biomater.* 2018
712 Mar;69:323–31.
- 713 59. Allen AJ, Zhang F, Joseph Kline R, Guthrie WF, Ilavsky J. NIST Standard Reference
714 Material 3600: Absolute Intensity Calibration Standard for Small-Angle X-ray
715 Scattering. *J Appl Crystallogr.* 2017;50:462–74.
- 716 60. Turunen MJ, Khayyeri H, Guizar-Sicairos M, Isaksson H. Effects of tissue fixation and
717 dehydration on tendon collagen nanostructure. *J Struct Biol.* 2017 Sep;199(3):209–15.
- 718 61. Khayyeri H, Blomgran P, Hammerman M, Turunen MJ, Löwgren A, Guizar-Sicairos M,
719 Aspenberg P, Isaksson H. Achilles tendon compositional and structural properties are
720 altered after unloading by botox. *Sci Rep.* 2017 Dec 12;7(1):13067.
- 721 62. Barth HD, Zimmermann EA, Schaible E, Tang SY, Alliston T, Ritchie RO.
722 Characterization of the effects of x-ray irradiation on the hierarchical structure and
723 mechanical properties of human cortical bone. *Biomaterials.* 2011;32(34):8892–904.
- 724 63. Duck FA. Mechanical Properties of Tissue. *Phys Prop Tissues.* 1990;3:137–65.
- 725 64. Ker RF. DYNAMIC TENSILE PROPERTIES OF THE PLANTARIS TENDON OF
726 SHEEP (OVIS ARIES). Vol. 2, *exp. Biol.* 1981.
- 727